International Journal of
Molecular Sciences

MDPI

Article

Antioxidant Chimeric Molecules: Are Chemical Motifs Additive? The Case of a Selenium-Based Ligand

Davide Zeppilli [1,†], Anna Aldinio-Colbachini [2], Giovanni Ribaudo [3,†], Cristina Tubaro [1], Marco Dalla Tiezza [1], Marco Bortoli [4], Giuseppe Zagotto [5] and Laura Orian [1,*]

[1] Dipartimento di Scienze Chimiche, Università degli Studi di Padova, Via Marzolo 1, 35131 Padova, Italy
[2] CNRS, Aix Marseille Université, BIP, IMM, IM2B, 31 Chemin J. Aiguier, 13009 Marseille, France
[3] Dipartimento di Medicina Molecolare e Traslazionale, Università degli Studi di Brescia, Viale Europa 11, 25123 Brescia, Italy
[4] Hylleraas Centre for Quantum Molecular Sciences, Department of Chemistry, University of Oslo, 0315 Oslo, Norway
[5] Dipartimento di Scienze del Farmaco, Università degli Studi di Padova, Via Marzolo 5, 35131 Padova, Italy
* Correspondence: laura.orian@unipd.it; Tel.: +39-049-8275140
† These authors contributed equally to this work.

Abstract: We set up an in silico experiment and designed a chimeric compound integrating molecular features from different efficient ROS (Reactive Oxygen Species) scavengers, with the purpose of investigating potential relationships between molecular structure and antioxidant activity. Furthermore, a selenium centre was inserted due to its known capacity to reduce hydroperoxides, acting as a molecular mimic of glutathione peroxidase; finally, since this organoselenide is a precursor of a N-heterocyclic carbene ligand, its Au(I) carbene complex was designed and examined. A validated protocol based on DFT (Density Functional Theory) was employed to investigate the radical scavenging activity of available sites on the organoselenide precursor ((SMD)-M06-2X/6-311+G(d,p)//M06-2X/6-31G(d)), as well as on the organometallic complex ((SMD)-M06-2X/SDD (Au), 6-311+G(d,p)//ZORA-BLYP-D3(BJ)/TZ2P), considering HAT (Hydrogen Atom Transfer) and RAF (Radical Adduct Formation) regarding five different radicals. The results of this case study suggest that the antioxidant potential of chemical motifs should not be considered as an additive property when designing a chimeric compound, but rather that the relevance of a molecular topology is derived from a chemical motif combined with an opportune chemical space of the molecule. Thus, the direct contributions of single functional groups which are generally thought of as antioxidants per se do not guarantee the efficient radical scavenging potential of a molecular species.

Keywords: antioxidant; DFT calculations; gold carbene complexes; ROS scavenging; selenium; structure reactivity

Citation: Zeppilli, D.; Aldinio-Colbachini, A.; Ribaudo, G.; Tubaro, C.; Dalla Tiezza, M.; Bortoli, M.; Zagotto, G.; Orian, L. Antioxidant Chimeric Molecules: Are Chemical Motifs Additive? The Case of a Selenium-Based Ligand. *Int. J. Mol. Sci.* **2023**, *24*, 11797. https://doi.org/10.3390/ijms241411797

Academic Editor: Ming-Ju Hsieh

Received: 2 July 2023
Revised: 18 July 2023
Accepted: 19 July 2023
Published: 22 July 2023

1. Introduction

The cellular redox balance, that is, the intracellular balance of pro-oxidant and antioxidant species, is finely tuned in living beings. The deterioration of this equilibrium condition leads to oxidative stress, which is characterised by an excess of harmful free radicals [1]. It is noteworthy that these chemical species containing one or more unpaired electrons [1] are physiologically generated in biological systems, e.g., during the oxidative phosphorylation [2] or by fundamental enzymes such as cytochrome P450, mainly in the form of reactive nitrogen species (RNS) and reactive oxygen species (ROS) [3]. ROS, e.g., hydroxyl radicals ($^{\bullet}OH$), superoxide anion radicals ($^{\bullet}O_2^-$) and hydroperoxyl radicals ($^{\bullet}OOR$), are the most dangerous and contribute to severe injury [4]. Their accumulation leads to nucleic acid damage, protein modification and lipid peroxidation and has been associated with the onset and progression of several pathological conditions, e.g., neurodegenerative

disorders [5], cardiovascular diseases [6] and some types of cancer [7], as well as mood disorders [8] and schizophrenia [9].

Antioxidants can contrast with oxidative stress by inhibiting radical-promoted oxidation processes [10]. They can be classified as endogenous and exogenous systems. In the former group, we find enzymes such as superoxide dismutase (SOD), glutathione peroxidase (GPx) and catalase. While SODs convert $^{\bullet}O_2^-$ into H_2O_2 and H_2O [11], GPxs [12,13] and catalases [14] transform hydroperoxides into nonradical, nonreactive and thermally stable products [15]. Among endogenous antioxidants, there are also some molecular systems, such as glutathione (GSH) [16] and melatonin [17], which exert their action by scavenging the radicals. This capacity is also found in exogenous antioxidants, which are mostly natural substances introduced with food. They include phenolic compounds, such as flavonoids [18], and dietary molecules, like tocopherols [19], carotenoids [20], omega-3 fatty acids [21], coenzyme Q10 [22], N-acetylcysteine [23], ginkgolides and bilobalide [24] and ascorbic acid [25]. In fact, in recent years, various epidemiological studies have correlated the consumption of antioxidant dietary compounds in humans with a reduced risk of developing diseases related to oxidative stress [26,27]. Interestingly, accumulating evidence also ascribes their cellular effects to their potential for modulating intracellular signalling pathways [28–31], key proteins' activity [32] and genes [33,34], as well as the gut microbiota [34,35].

All these indications have inspired physicians to complement standard therapies with antioxidant treatments for a wide range of disorders, to improve quality of life and try to slow the progression of their pathologies [36–38]. It is also worth noting that the central nervous system (CNS) is particularly vulnerable to oxidative stress, due to its high oxygen consumption, and antioxidant supplements can also improve patient conditions in the presence of mood disorders and dependencies [39,40]. As further evidence for this assessment, the great effectiveness of some drugs historically used for the treatment of CNS diseases has been linked to their ability to mitigate oxidative stress as a sub action of their primary pharmacological activity [41]. As proved by in silico studies, examples are the popular fluoxetine (better known by its commercial name, Prozac), a selective serotonin reuptake inhibitor (SSRI) used mainly as an antidepressant [42–44], and zolpidem (2, Scheme 1), a $GABA_A$ receptor agonist belonging to the class of imidazopyridines, which acts as a sedative and hypnotic [45]. For the latter, the effectiveness was recently also experimentally proved by Yousefsani et al. [46]. Despite numerous in vitro and in vivo studies, the consequences of most antipsychotics and antidepressants on the cellular redox balance are still controversial and the collection of works investigating their antioxidant properties at the molecular level is scarce [41]. Therefore, research is needed to validate the proof of concept linking the complex aetiology of CNS disorders to the need for polypharmacological agents with enhanced antioxidant activity. A strategy to move forward relies on new approaches for the unambiguous characterisation of well-known drugs, together with the rational design of new drug candidates.

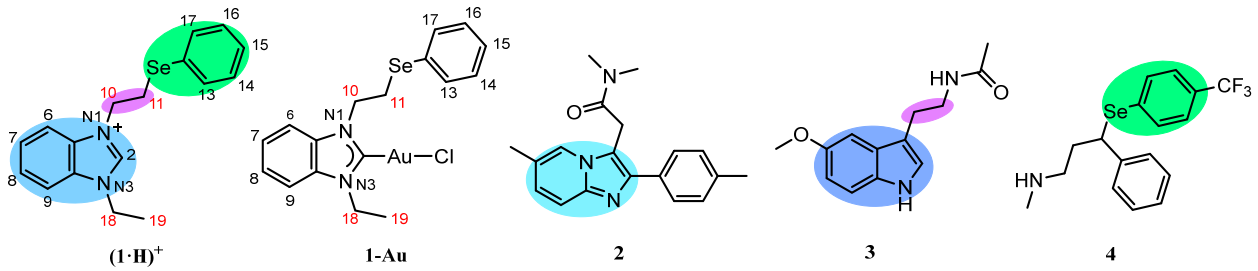

Scheme 1. Chemical structures of the chimeric pro-ligand $(1{\cdot}H)^+$, the NHC-Au(I) complex (1-Au), zolpidem (2), melatonin (3) and selenofluoxetine (4). Red numbers indicate sites from which HAT may occur; black numbers indicate that RAF may occur.

Computational techniques are a green, time and cost-saving tool to screen and rationalise the properties and mechanisms of molecular compounds. More than 70 commercialised drugs include some form of in silico study [47]. In particular, quantum chemistry calculations provide detailed structural, thermodynamic, and kinetic information on the elementary yet fundamental chemical reactions, but due to their computational burden and complexity, they are employed on highly specific and limited occasions in the drug discovery field. This is the case for numerous natural antioxidant substances [48], but also for bioinspired molecular compounds such as organoselenides, which are mimics of glutathione peroxidase (GPx) [49–51]. Density functional theory (DFT) methods are mostly used in these analyses because of their well-known accuracy at moderate computational cost. Unravelling the mechanistic features and energetics of the elementary reactions in which antioxidant activity is rooted is crucial to a rational approach to molecular design.

In this work, we seek to investigate whether and to what extent the chemical motifs of well-known antioxidants are additive. Taking inspiration from drugs and natural compounds with known antioxidant properties, we designed a benzimidazole scaffold 'decorated' at position N3 with an ethyl group, and at position N1 with a group containing a selenium centre and a phenyl ring ($(1{\cdot}H)^+$, Scheme 1). The $(1{\cdot}H)^+$ was used as a precursor of the N-heterocyclic carbene (NHC) Au(I) complex 1-Au (Scheme 1). The reactivity of cation $(1{\cdot}H)^+$ and 1-Au was characterised according to a state-of-the-art computational protocol based on DFT calculations [44,45,52]. The radical scavenging activity of all available sites was investigated considering HAT (Hydrogen Atom Transfer) towards five different radicals ($^{\bullet}OH$, $^{\bullet}OCH_3$, $^{\bullet}OOH$, $^{\bullet}OOCH_3$, $^{\bullet}OOCH{=}CH_2$) and RAF (Radical Adduct Formation) with the hydroxyl radical; the capacity of the selenium centre to reduce hydrogen peroxide was also estimated.

2. Results and Discussion

2.1. Rational Design of the Chimeric Compound

The characteristics of $(1{\cdot}H)^+$ were rationally chosen; the chimera consists of (i) a benzimidazole disubstituted with (ii) an ethyl group and (iii) a group containing a selenium centre. (i) The benzimidazole derivatives are clinically relevant as potential therapeutic agents for a wide range of disorders [53], including neurodegenerative diseases (e.g., Parkinson's [54] and Alzheimer's [55]). Since its discovery in 1944, the benzimidazole moiety has been used as a scaffold to synthesise a wide variety of compounds involved in biological processes. In the literature, many examples show antioxidant properties and a neuroprotective role [56,57]. Structure activity relationship (SAR) studies highlight the importance of the choice in tuning benzimidazole-based molecules to specific actions [58]. A similar motif formed by two condensed rings is present in zolpidem (2, Scheme 1) and in melatonin (3, Scheme 1). (ii) In $(1{\cdot}H)^+$, the nitrogen substituents were selected to enhance the ROS scavenging properties of the molecule, mainly through the HAT mechanisms, as shown in previous studies [59,60]. The chain with two methylene groups was chosen because it is closely analogous to 3, the compound in which it contains the most reactive site for the scavenging activity. In 2, the aromatic scaffold is connected to the nitrogen atom through two carbon atoms, one of which is involved in the amide bond. Indeed, also in 2, the methylene group at this level is the most reactive site [45]. This spacer is also common in other CNS drugs, such as fluoxetine or 4. (iii) The selenium atom was inserted in the system because of its capacity to reduce hydroperoxides [61]. In the last 40 years, many studies have proved the importance of selenium-based chemistry for human redox balance [62,63]. Selenocysteine is the key residue in the mechanism of action of several redox enzymes, including five different GPxs, thioredoxin reductases, methionine sulfoxide reductase and iodothyronine deiodinase [15]. This evidence continuously inspires the design and study of selenium-based organochalcogenides acting as GPx mimics; the most popular is ebselen (2-phenyl-1,2-benzisolenazol-3(2H)-one) [49], a selenenylamide which has been used in different clinical trials. Recently, the inclusion of one atom of selenium in fluoxetine was reported to improve its antioxidant properties [43].

Finally, $(1{\cdot}H)^+$ may be a precursor of a NHC ligand: the loss of the proton in C_2 allows the formation of transition metal complexes such as the Au(I) complex 1-Au (Scheme 1). Functional NHC ligands and their gold(I) complexes are currently the subject of intense investigation in medicinal chemistry as anticancer drugs [64–67]. In this regard, the incorporation of -SeR moieties into gold(I) NHC complexes may provide compounds capable of exerting a dual action on cancer cells. Azolium salts functionalised with -SeR moieties in the pendant nitrogen group and the corresponding metal complexes are already reported in the literature, but the number of studies is still limited [68–76].

The reactivity of $(1{\cdot}H)^+$ was investigated in silico; its potential energy surface was explored considering two different scavenging mechanisms, hydrogen atom transfer (HAT) and radical adduct formation (RAF). Both reaction mechanisms have been characterised thermodynamically and kinetically. In addition, we have investigated the hydrogen-peroxide-reducing capability of the selenide. To point out how the presence of environments of different polarity might influence the energetics of the HAT/RAF processes, $(1{\cdot}H)^+$ has been studied in the gas phase, water and benzene.

First, the geometry of $(1{\cdot}H)^+$ was fully optimised in the gas phase. Selected bond angles and lengths are shown in Figure 1. In particular, the imidazole and benzene rings are stacked in this structure. We confirmed that this arrangement corresponds to the lowest energy minimum with a scan analysis of the dihedral N1-C10-C11-Se.

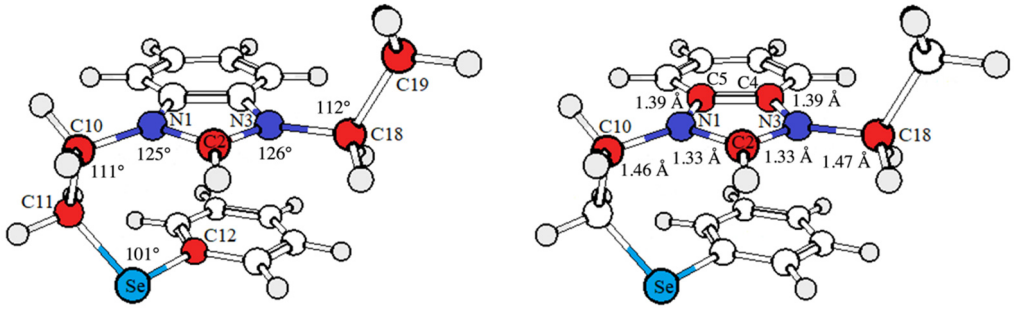

Figure 1. Fully optimised structure of $(1{\cdot}H)^+$ showing the most relevant bond angles and lengths; the atoms used in the measurements have been highlighted with colours for clarity, i.e., C (red), N (blue), Se (cyan). Level of theory: M06-2X/6-31G(d).

2.2. HAT Scavenging Mechanism of $(1{\cdot}H)^+$

Hydrogen atom transfer (HAT) is a concerted transfer of a hydrogen atom [77], i.e., $^\bullet$H, in a single kinetic step, from an H atom donor (e.g., (H_nL^+)) to an acceptor (e.g., a ROS ($^\bullet$R)), according to Equation (1):

$$H_nL^+ + {}^\bullet R \rightarrow H_{n-1}L^{\bullet +} + HR \quad (1)$$

In this work, we have considered five ROSs ($^\bullet$R = $^\bullet$OH, $^\bullet OCH_3$, $^\bullet$OOH, $^\bullet OOCH_3$, $^\bullet OOCH{=}CH_2$). The hydroxyl radical ($^\bullet$OH) is the most electrophilic and reactive among the oxygen-centred radicals, with a half-life of $\sim 10^{-9}$ s [78]; its high reactivity is accompanied by a low selectivity. Since metal ions, particularly iron, are widely present in biological systems, $^\bullet$OH formation is mainly attributed to the so-called iron-catalysed Haber–Weiss reaction [79,80], which makes use of Fenton chemistry ($H_2O_2 + {}^\bullet O_2^- \xrightarrow{Fe^{3+}} OH^- + {}^\bullet OH + O_2$). In cellular environments, oxy radicals [81] are also present. The simplest is the methoxy radical ($^\bullet OCH_3$). Peroxyl radicals (such as $^\bullet$OOH; $^\bullet OOCH_3$; $^\bullet OOCH{=}CH_2$) are less reactive species, capable of diffusing to remote cellular locations; their half-lives are of the order of seconds [82]. $^\bullet$OOH and $^\bullet OOCH_3$ were also chosen because they are the peroxyl analogues of $^\bullet$OH and $^\bullet OCH_3$; $^\bullet OOCH{=}CH_2$ is used as a mimic of lipid peroxyl radicals.

The thermodynamics of the HAT mechanism were investigated first because they reveal the feasibility of the reactions. All available sites of $(1{\cdot}H)^+$ were screened (see Scheme 1 for numbering). Since the direction from which the radical might arrive and react

is not predictable, multiple hydrogens belonging to the same site were considered (different H on the same C atom is indicated with α, β, γ). The Gibbs free reaction energies (ΔG°_{HAT}) computed in the gas phase and in two different solvents, i.e., water and benzene, are shown in Figure 2; the reaction energies of the most reactive sites are reported in Table S1.

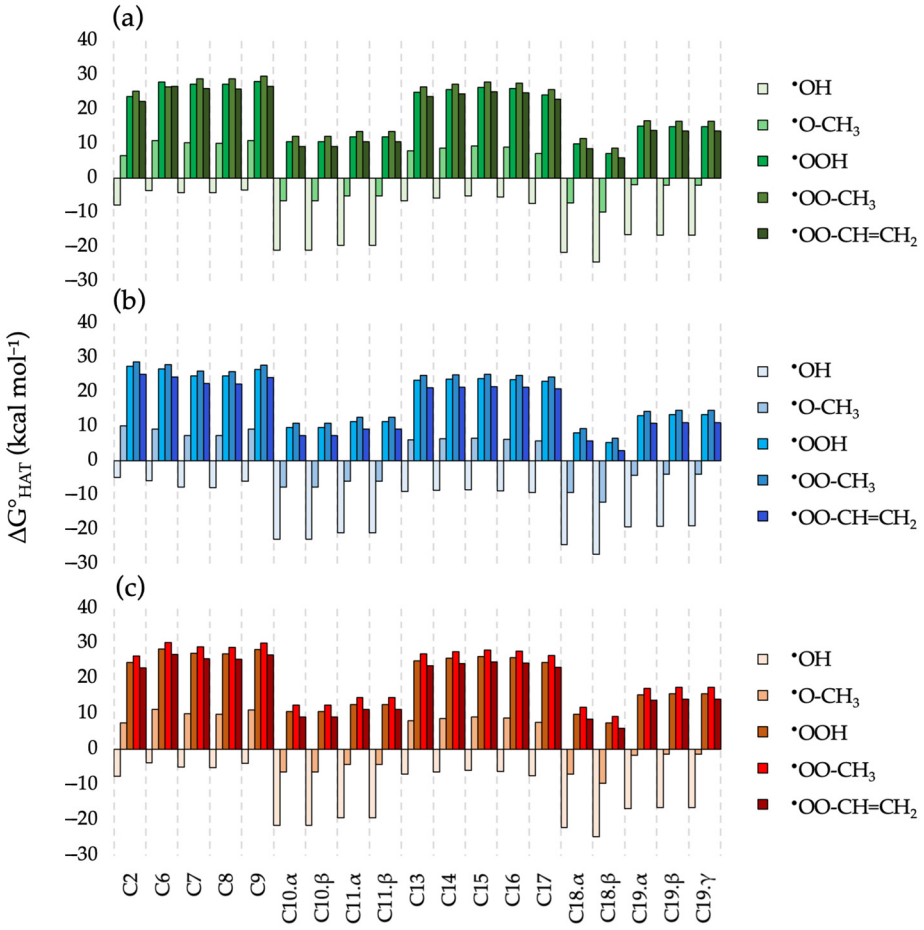

Figure 2. ΔG°_{HAT} (kcal mol^{-1}) in gas phase (**a**), in water (**b**) and in benzene (**c**) for the scavenging of $^{\bullet}$OH, $^{\bullet}$OCH$_3$, $^{\bullet}$OOH, $^{\bullet}$OOCH$_3$ and $^{\bullet}$OOCH=CH$_2$ via HAT from all the available sites of $(1{\cdot}H)^+$. Level of theory: (SMD)-M06-2X/6-311+G(d,p)//M06-2X/6-31G(d).

All reactions with the hydroxyl radical in the gas phase (Figure 2a) were exergonic, with ΔG°_{HAT} values in the range of −24.33 to −3.56 kcal mol^{-1}. Only the most reactive sites (C10, C11, C18, C19) showed a certain reactivity with the methoxy radical; their ΔG°_{HAT} values were in the range –9.83 to 1.86 kcal mol^{-1}. The other reactions with $^{\bullet}$OCH$_3$, as well as all reactions with hydrogen peroxyl, methyl peroxyl and the lipid peroxyl radicals, were strongly endergonic and thus thermodynamically unfavoured. The values were in the range of 7.26 to 28.12 kcal mol^{-1} ($^{\bullet}$OOH), 8.86 to 29.71 kcal mol^{-1} ($^{\bullet}$OOCH$_3$) and 5.97 to 26.82 kcal mol^{-1} ($^{\bullet}$OOCH=CH$_2$), respectively. C10, C11, C18 and C19, i.e., the alkyl sites inserted in $(1{\cdot}H)^+$ to mimic the most reactive sites in melatonin and zolpidem, were seen to have much lower ΔG°_{HAT} then the aromatic sites. Overall, C18 was the most reactive site for scavenging through the HAT mechanism for all radicals. When different hydrogens belong to the same site, they show similar reactivity. The greatest dissimilarity was found for C18.α and C18.β; the latter was systematically more favoured by ~3 kcal mol^{-1}. The reason for this difference is probably due to steric effects; in both radicals, the C2-N3-C18-C19 dihedral was almost planar but, in the most stable configuration, it had a value close to 0°, positioning the C19 methyl group on the free side of C2. In contrast, in the other configuration, the dihedral was near 180° and the methyl group was closer to the benzene ring; thus, the steric hindrance was greater. In water (Figure 2b), an appreciable stabilisation

of the products occurred, while in benzene (Figure 2c) the values were very close to those computed in the gas phase; thus, the trends in the gas phase were also maintained in solvent. Only in the case of C2 does the HAT mechanism generate a product which is more stable in the gas phase and in benzene than in water.

A kinetic analysis of the HAT reaction from each site was carried out in the gas phase, water and benzene (Table 1). In the gas phase, activation barriers spanned a range that reached 5.71 kcal mol^{-1} in the case of C11.β. In water and benzene, this value was seen to be higher, with the least favourable reactions being at C10.β for both solvent media with an activation energy of 4.69 and 5.32 kcal mol^{-1}, respectively. HAT from site C11.α had the lowest barrier in all conditions. In the gas phase, the TS had a lower energy than the free reactants (the calculated barrier with respect to the reactant complex was 5.47 kcal mol^{-1}), whereas in water and benzene very low barriers of 1.39 and 0.16 kcal mol^{-1} were computed. Interestingly, the most kinetically favoured reactions (C11.α, C19.γ) did not correspond to the most thermodynamically favoured ones (C18). Generally, the trends for the different sites were the same in all three conditions (the coordinates of the HAT radical products and the transition states are reported in Table S5 and Table S6).

Table 1. ΔG_{HAT} (kcal mol^{-1}) of transition state (TS) and free products (P) in the gas phase, water and benzene for the scavenging of •OH via HAT from the most reactive sites of $(1{\cdot}H)^+$. The values are given with respect to the free reactants (R). Level of theory: (SMD)-M06-2X/6-311+G(d,p)//M06-2X/6-31G(d).

	$\Delta G_{HAT,\ gas\ phase}$ (kcal mol^{-1})								
	C10.α	**C10.β**	**C11.α**	**C11.β**	**C18.α**	**C18.β**	**C19.α**	**C19.β**	**C19.γ**
R	0.00	0.00	0.00	0.00	0.00	0.00	0.00	0.00	0.00
TS	2.33	4.07	−0.88 *	5.43	3.55	1.40	3.48	5.71	0.83
P	−20.98	−20.97	−19.57	−19.57	−21.59	−24.3	−16.4	−16.55	−16.6
	$\Delta G_{HAT,\ water}$ (kcal mol^{-1})								
R	0.00	0.00	0.00	0.00	0.00	0.00	0.00	0.00	0.00
TS	2.38	5.32	1.39	3.89	2.97	3.35	2.61	2.93	2.49
P	−22.74	−22.73	−20.95	−20.95	−24.29	−27.1	−19.2	−18.94	−18.9
	$\Delta G_{HAT,\ benzene}$ (kcal mol^{-1})								
R	0.00	0.00	0.00	0.00	0.00	0.00	0.00	0.00	0.00
TS	2.32	4.69	0.16	4.59	3.53	2.34	3.31	4.40	1.93
P	−21.39	−21.38	−19.32	−19.32	−22.06	−24.62	−16.64	−16.39	−16.38

* The barrier calculated with reference to the reactant complex is 5.47 kcal mol^{-1} [83].

These results can be compared with those obtained for 2, 3 and 4, which inspired the molecular structure of $(1{\cdot}H)^+$. The thermodynamic data of the HAT mechanism for these three compounds were calculated in a previous work by some of us with the same level of theory employed here [42,45]; thus, a quantitative comparison is possible. Their most reactive sites were inserted into the chemical scaffold of $(1{\cdot}H)^+$ and are still associated with the most favoured HAT reactions. However, the great exergonicity of HAT in 2, 3 and 4 ($\Delta G^{\circ}_{HAT} < -30$ kcal mol^{-1} for the scavenging of •OH) was poorly reproduced in $(1{\cdot}H)^+$ and the ability to quench peroxyl radicals was completely lost. In other words, the radical products of $(1{\cdot}H)^+$ were not as stabilised as in the parent molecules. This outcome can be rationalised by inspecting the electronic structure of the radical products. Figure 3 shows the spin densities of the most stable radical products formed by HAT from $(1{\cdot}H)^+$, 2, 3 and 4. In the parent molecules, the unpaired electron was delocalised on the aromatic ring adjacent to the reaction site, particularly in zolpidem. In contrast, in the selected radicals of $(1{\cdot}H)^+$ (C18.α and C11.α), the spin densities were essentially localised in the carbon atom which had lost the hydrogen atom. In particular, the reactivity of the methylene group in C18 decreased in $(1{\cdot}H)^+$ due to a smaller delocalisation in the aromatic ring. Not even the presence of the Se nucleus seemed to improve the scavenging activity of $(1{\cdot}H)^+$, since there

was no aromatic ring on which the spin density can be delocalised, like in 4. Scheme 2 shows how the unpaired electron is delocalised in a 4-like compound using resonance structures, according to the result of the spin density. The delocalisation involves the entire aromatic ring; therefore, in the absence of a direct phenyl group, the unpaired electron remained localised on a single carbon atom, as in $(1{\cdot}H)^+$. This is clear evidence that the effectiveness of an antioxidant moiety in HAT is not governed by the sole chemical nature of the atom involved in the transfer, but also requires a favourable extended structure that can efficiently delocalize the newly formed radical. Thus the 'blind' addition of multiple favourable HAT sites, taken from different scavengers, not only does not result in an overall better antioxidant, but could also perform worse than the distinct parent molecules.

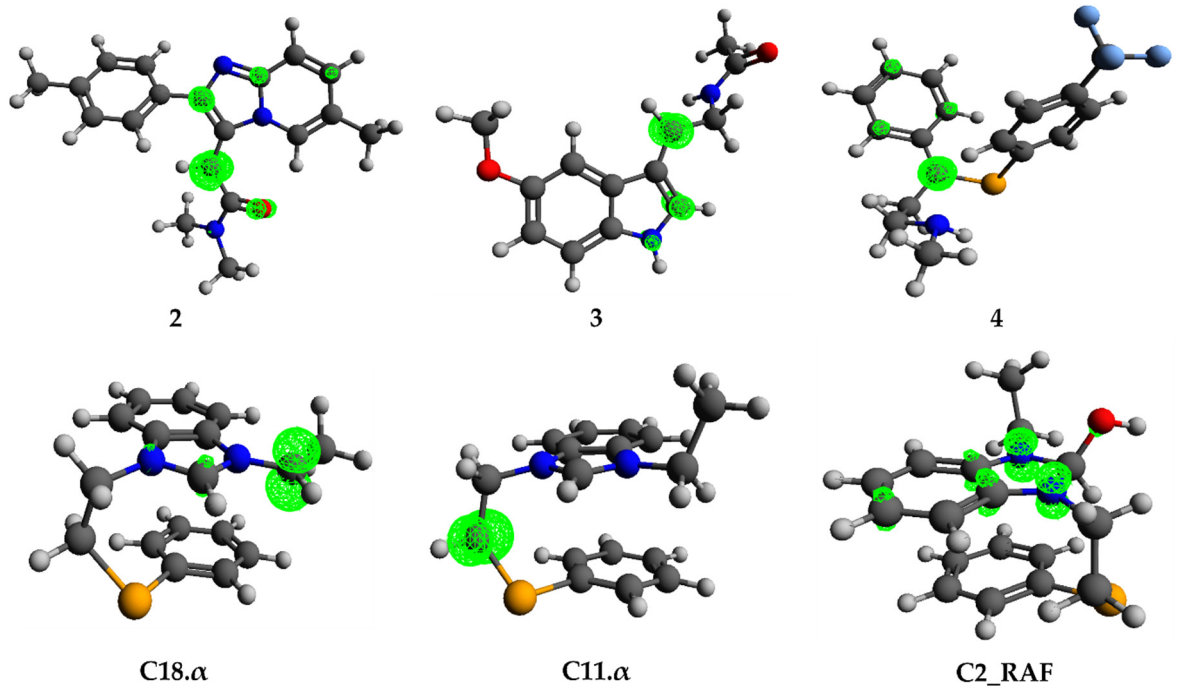

Figure 3. Spin densities on the radical products of 2, 3, 4 (when HAT occurs from the most reactive site) [42,45] and $(1{\cdot}H)^+$ when HAT occurs from C18.α and C11.α, and when RAF occurs from C2. Isodensity value of 0.015. Level of theory: M06-2X/6-311+G(d,p)//M06-2X/6-31G(d).

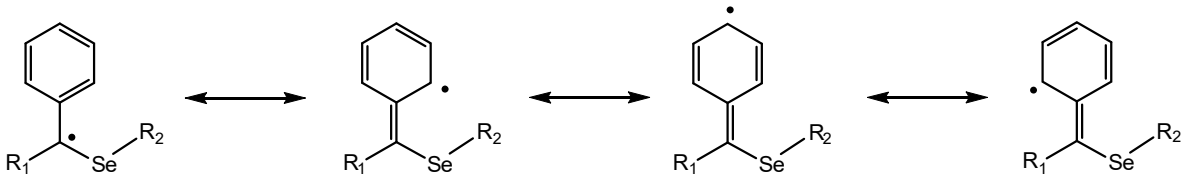

Scheme 2. Resonance structures for the HAT radical product of a 4-like chemical structure.

2.3. RAF Scavenging Mechanism of $(1{\cdot}H)^+$

Radical adduct formation (RAF) is a key scavenging mechanism for molecules characterised by unsaturated bonds: electrophilic radicals are more likely to be involved in RAF reactions than non-electrophilic ones. The mechanism for a general scavenger (H_nL^+) is shown in Equation (2):

$$H_nL^+ + {}^{\bullet}R \rightarrow [H_nL{-}R]^{\bullet+} \quad (2)$$

RAF was only investigated for the hydroxyl radical. First, the thermodynamic viability of RAF reactions was determined for all the available sites (see Scheme 1). Specifically, RAF from the C6, C7, C8 and C9 sites depends on where the radical attack occurs, that is, above or under the benzimidazole plane, generating two chiral products. Gibbs free reaction

energies (ΔG°_{RAF}) were calculated for all stereoisomers. All the ΔG°_{RAF}, calculated in the gas phase and in two different solvents, that is, water and benzene, are shown in Figure 4. The reaction energies of the most reactive sites (C2, C6, C9) are also reported in Table S2. All reactions are exergonic regardless of the environment.

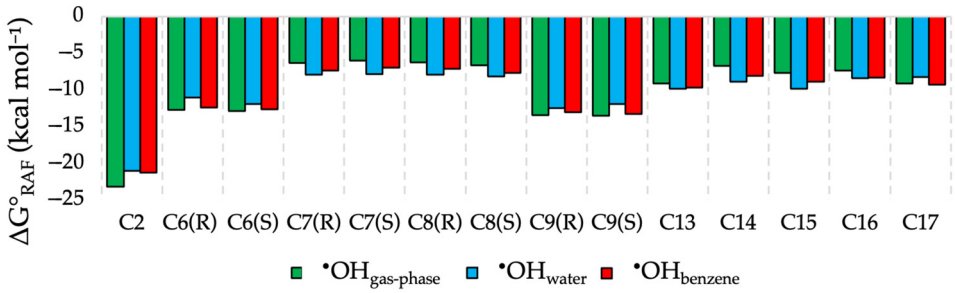

Figure 4. ΔG°_{RAF} (kcal mol^{-1}) in gas phase (green), in water (light blue) and in benzene (red) for the scavenging of •OH through RAF from all the available sites of $(1{\cdot}H)^+$. Level of theory: (SMD)-M06-2X/6-311+G(d,p)//M06-2X/6-31G(d).

Focusing on the most reactive sites, an appreciable stabilisation of the product is predicted in the gas phase (with ΔG°_{RAF} in the range −23.17 to −13.46 kcal mol^{-1}) and in benzene versus water. Chiral products from the same reaction site have similar Gibbs free energies. The ΔG°_{RAF} values for the most reactive site (C2) were slightly more negative than the most favoured ones obtained for the HAT mechanism. The high reactivity via RAF from C2 can be explained by analysing the spin density of the radical product (Figure 3). In this radical, the spin density was delocalised on the two condensed rings, explaining its stability. Nevertheless, this delocalisation was not sufficient to provide the same scavenging potential predicted for 2, 3 and 4 via HAT from their most reactive sites.

The transition states energies for RAF from C2 were calculated in the gas phase, water and benzene (the results are summarised in Table 2). Activation energies were found to be the lowest in the gas phase, as was the case for reaction energies. The energy barriers were close to those calculated for the scavenging mechanism via HAT from C19.γ and C18.β, indicating that both mechanisms may operate with the same probability at different sites of the molecule.

Table 2. ΔG_{RAF} (kcal mol^{-1}) of transition state (TS) and free products (P) in gas phase, water and benzene for the scavenging of •OH via RAF from the most reactive site of $(1{\cdot}H)^+$ (C2). The values are given with respect to the free reactants (R). Level of theory: (SMD)-M06-2X/6-311+G(d,p)//M06-2X/6-31G(d).

	ΔG_{RAF} (kcal mol^{-1})		
	Gas Phase	**Water**	**Benzene**
R	0.00	0.00	0.00
TS	1.17	1.63	2.21
P	−23.17	−19.13	−19.35

The characterisation of $(1{\cdot}H)^+$ was completed by analysing the oxidation properties of the selenium centre. According to the literature, in the presence of hydroperoxides, selenides are mainly oxidised to selenoxides [61]; thus, a such reaction was investigated (Scheme 3).

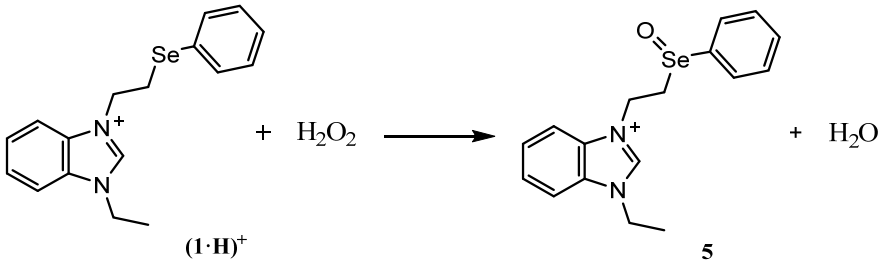

Scheme 3. Oxidation of $(1{\cdot}H)^+$ by hydrogen peroxide with the formation of the selenoxide 5 and water.

Free reaction energies (ΔG_{ox}) were calculated in the gas phase, water and benzene. In the gas phase, the barrier ($\Delta G^{\ddagger}_{ox}$) reached 48.87 kcal mol^{-1}, while the stabilised P lay at −17.47 kcal mol^{-1}. The reaction was undoubtedly thermodynamically favoured, but the activation energy value indicated that it is kinetically unfeasible under standard conditions. The trend in the gas phase was maintained in solution, where the reaction was more favoured both thermodynamically and kinetically. In benzene, the barrier was 47.24 kcal mol^{-1} and the energy of the free products was −22.19 kcal mol^{-1}. An appreciable stabilisation of both TS ($\Delta G^{\ddagger}_{ox}$ = 38.80 kcal mol^{-1}) and P (ΔG_{ox} = −35.08 kcal mol^{-1}) was observed in water. These findings show that the presence of Se alone is not enough to grant an effective peroxide-reducing molecule, and a more tailored design of the chemical environment around the Se atom is necessary to arrive at a functional molecule.

2.4. HAT Scavenging Mechanism of 1-Au

The geometry of 1-Au was fully optimised and the selected bond angles and lengths are shown in the Supporting Information (Figure S1). A conformational analysis based on rotation about the N1-C10-C11-Se dihedral angle revealed that, like in $(1{\cdot}H)^+$, this structure is stabilised by dispersive inter-ring π–π interaction (Supporting Information, Figure S2).

As well as for $(1{\cdot}H)^+$, the capacity of scavenging through the HAT mechanism has also been investigated for 1-Au, to establish where and how the presence of gold influences the reactivity of the complex. Once again, the thermodynamic viability of the HATs was investigated first. All possible sites which might react via HAT have been screened (see Scheme 1 for numbering). Electronic reaction energies (ΔE°_{HAT}) computed in the gas phase, water, and benzene are shown in Figure 5; the reaction energies of the most reactive sites are also reported in Table S3. Due to the presence of the metal centre and, therefore, the need to use a different level of theory for molecular optimisations, obtaining thermodynamic corrections would require the combination of two different functionals in order to be consistent with the level of theory used for the pro-ligand's HAT. This approach could worsen the accuracy of the final results; hence, no Gibbs free reaction energies are reported for the mechanism of 1-Au.

The data of the gas phase (Figure 5a) show that all the reactions with the hydroxyl radical are thermodynamically favoured, as predicted for $(1{\cdot}H)^+$, with ΔE°_{HAT} in the range of −14.43 to –2.14 kcal mol^{-1}. The most reactive sites with $^{\bullet}$OH (C10.α, C11.α) showed a weak reactivity with the methoxy radical; their ΔE°_{HAT} values were in the range of −1.56 to −0.88 kcal mol^{-1}. On the other hand, the remaining reactions with $^{\bullet}OCH_3$, as well as all reactions with the peroxyl radicals, were strongly endergonic and, thus, thermodynamically disfavoured. The values ranged from 16.70 to 28.99 kcal mol^{-1} ($^{\bullet}$OOH), 18.75 to 31.03 kcal mol^{-1} ($^{\bullet}OOCH_3$) and 15.93 to 28.22 kcal mol^{-1} ($^{\bullet}OOCH{=}CH_2$). When multiple hydrogens are on the same site, they have different tendencies to react (with the exception of the C19 site). HAT from C10.α, C11.α and C18.α sites were ∼6, ∼5 and ∼1 kcal mol^{-1} more favoured than their β correspondents, respectively. Therefore, the presence of a gold atom in the molecule actually modifies the reactivity of the organic part compared to the parent pro-ligand; in fact, all hydrogens labelled with α were further from the metal centre than their β correspondents. In particular, the reactivity of HAT of 1-Au was much lower than $(1{\cdot}H)^+$; the ΔE°_{HAT} for the most reactive sites of 1-Au were much

less negative than the ΔE°_{HAT} of $(1{\cdot}H)^{+}$ (Supporting Information, Table S4). Moreover, the most reactive site for RAF (C2) was completely lost, due to coordination with Au(I).

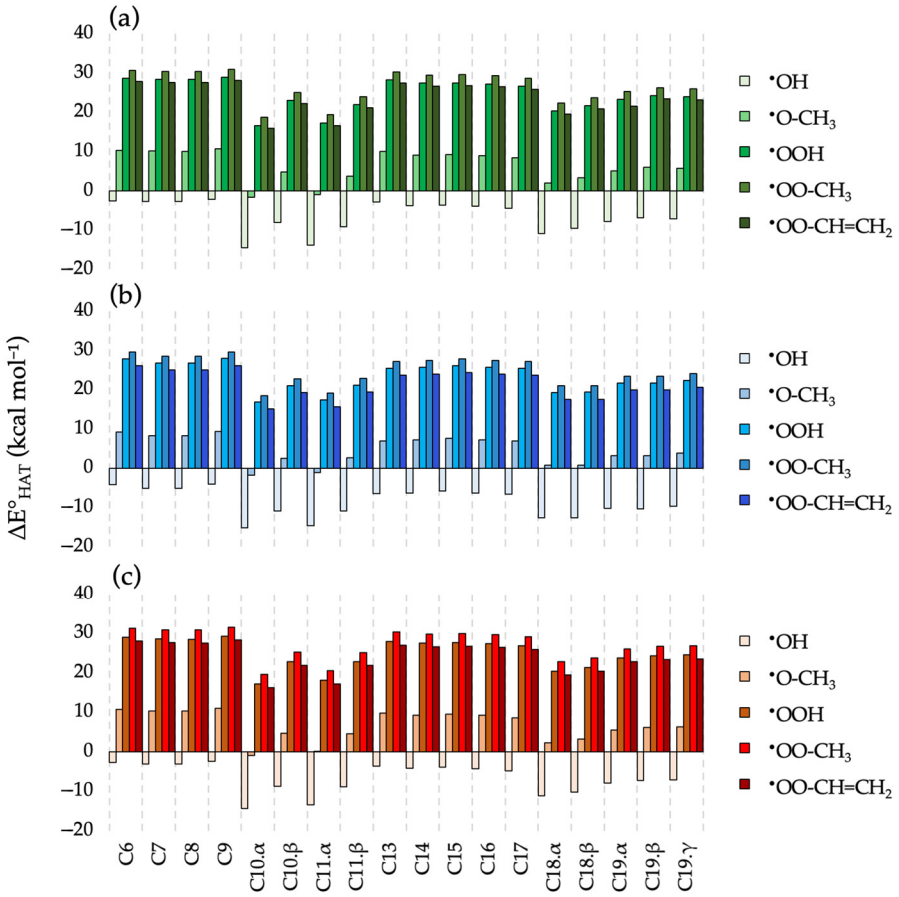

Figure 5. ΔE°_{HAT} (kcal mol^{-1}) in gas phase (**a**), in water (**b**) and in benzene (**c**) for the scavenging of •OH, •OCH$_3$, •OOH, •OOCH$_3$ and •OOCH=CH$_2$ via HAT from all the available sites of 1-Au. Level of theory: (SMD)-M06-2X/SDD (Au), 6-311+G(d,p)//ZORA-BLYP-D3(BJ)/TZ2P.

As a general rule, in water (Figure 5b), a notable stabilisation of the products was observed (with ΔE°_{HAT} in the range of –15.15 to –4.04 kcal mol^{-1} for the removal of •OH), while in benzene (Figure 5c), the values were very close to those computed in the gas phase (with ΔE°_{HAT} in the range of –14.31 to –2.34 kcal mol^{-1} for the removal of •OH). The trends in the gas phase were maintained in the presence of solvent, with the exception, in water, of C18, where both α and β sites had the same reactivity.

3. Materials and Methods

All the systems have been described at the same level of theory, except for the Au(I) complex (see below). In the absence of metal, the density functional theory (DFT) calculations were performed using Gaussian16 [84]. Full geometry optimisations were carried out using the M06-2X functional [85] with a standard 6-31G(d), a double-ζ and single polarisation basis set (level of theory: M06-2X/6-31G(d)). Three single-point energy calculations were then carried out to better estimate the electronic energies. The first single point was run in gas phase, while in the remaining two cases the SMD (Solvation Model based on Density) model [86] was used to estimate solvation effects in two different media, that is, water and benzene, mimicking a polar and an apolar environment, respectively. The basis set in these single-point calculations was extended to a 6-311+G(d,p), which is a triple-ζ quality basis set supplemented with diffuse functions and includes a double polarisation function on each atom. This level of theory is referred to as: (SMD)-M06-2X/6-311+G(d,p)//M06-2X/6-31G(d).

The gold complex required a dedicated protocol, mainly due to the presence of the heavy metal centre; to accurately estimate its geometry, Amsterdam Density Functional (ADF) was used [87], which allows the employment of the Zeroth-order regular approximation (ZORA) to include relativistic effects in the calculations [88]. Full geometry optimisations were performed using the BLYP functional [89,90], with the inclusion of Grimme dispersion with the Becke–Johnson damping function [91,92]. The TZ2P basis set was used, that is, a large, uncontracted set of Slater-type orbitals of triple-ζ quality, augmented with two sets of polarisation functions per atom; furthermore, the small frozen core approximation was used (level of theory: ZORA-BLYP/TZ2P). Then, single-point calculations were carried out using the approach adopted for the pro-ligand described above. The only difference was the basis set associated with the gold atom, i.e., SDD [93] (Stuttgart–Dresden–Bonn optimised basis set and fully relativistic electronic core potential); the level of theory is indicated by (SMD)-M06-2X/SDD (Au), 6-311+G(d,p)//ZORA-BLYP-D3(BJ)/TZ2P.

Equilibrium and transition state geometries were optimised without symmetry constraints, using modern consolidated analytical gradient techniques. Frequency calculations were employed to calculate thermodynamic corrections at 298.15 K and 1 atm, and to verify the nature of all structures. Transition states were confirmed with the presence of a single imaginary frequency, whereas only real frequencies were computed for the minima. Spin contamination was checked for doublet ground-state species and was found to be negligible. Spin density surfaces were drawn for selected structures with Avogadro [94], with an isodensity value of 0.015.

4. Conclusions

This work aimed at the design of a chimeric molecule $(1{\cdot}H)^+$ structurally related to the well-known antioxidants 2, 3 and 4 with enhanced activity, e.g., capable of acting as a ROS scavenger via the HAT or RAF mechanisms, as well as being able to reduce hydroperoxides thanks to the presence of a selenium atom; furthermore, the presence of a Se atom could improve the overall scavenging activity, as was reported for fluoxetine and its analogous selenofluoxetine [42]. Finally, the design of the Au(I) carbene complex of $(1{\cdot}H)^+$ (1-Au) was employed to investigate the effect of the presence of this heavy metal centre on the scavenging activity, as well as on the capacity of selenium to reduce H_2O_2.

The results presented here, obtained in silico using state-of-the-art consolidated computational methodologies, suggest that the scavenging activity of $(1{\cdot}H)^+$ is overall lower than that of the parent molecules. In addition, the reactivity of the selenium centre was reduced in comparison to model phenyl alkyl selenides. Moreover, the transformation of the $(1{\cdot}H)^+$ ligand into a N-heterocyclic carbene through the addition of an Au atom in the structure resulted in less favourable reaction energies for the HAT mechanism, both in the gas-phase and in water, when compared to $(1{\cdot}H)^+$, and the loss of the most reactive site for RAF because of the coordination of C2 to Au.

Although in vitro reactivity tests are needed to fully clarify these predictions, this analysis clearly demonstrates the importance of a large molecular topology for the antioxidant mechanisms, as subtle structural changes imply significant variations in reactivity, which can be nicely rationalised with modern and high-performance computational protocols. In particular, the scavenging potential does not seem to be related to localised organic moieties, i.e., functional groups or residues, but is rather tuned by the chemical environment in which the reactive site is immersed. The size of this environment remains uncertain and deserves to be explored, as does the definition of antioxidant motifs which maintain their properties when inserted in a different chemical structure.

Overall, this study demonstrates the relevance of advanced computational techniques in guiding the rational design of antioxidant molecules. However, even if it may seem counterintuitive to some extent, the concept of antioxidant motifs should overcome that of functional groups. In fact, in the case study here presented, we showed that the contributions of different and chemically diverse antioxidant 'building blocks' were not additive, and this aspect should be considered when the rational design of an antioxidant compound

is approached, and also when using large scale methods such as those based on artificial intelligence. Thus, a wider, computer-guided exploration of chemical space may pave the way for the identification of synergistic interconnections between antioxidant motifs, and their definition and characterisation remains one of the challenges of contemporary rational drug design.

Supplementary Materials: The supporting information can be downloaded at: https://www.mdpi.com/article/10.3390/ijms241411797/s1.

Author Contributions: Conceptualization, G.R., C.T., M.B., G.Z. and L.O.; methodology, M.D.T., M.B. and L.O; validation, G.R., M.B. and L.O.; formal analysis, G.R., M.B. and L.O.; investigation, D.Z., A.A.-C. and M.D.T.; resources, L.O.; data curation, D.Z. and A.A.-C.; writing—original draft preparation, D.Z., A.A.-C. and G.R.; writing—review and editing, G.R., C.T., M.D.T., M.B., G.Z. and L.O.; visualization, D.Z. and A.A.-C.; supervision, L.O.; project administration, L.O.; funding acquisition, L.O. All authors have read and agreed to the published version of the manuscript.

Funding: This research was funded by the Università degli Studi di Padova. CINECA is acknowledged for the generous allocation of computational time (ISCRA project HP10CB3TNH "REdox state role in Bio-inspired ELementary reactions 2 (REBEL2); P.I.: L.O.).

Institutional Review Board Statement: Not applicable.

Informed Consent Statement: Not applicable.

Data Availability Statement: The data used are contained within the article or in the Supplementary Materials.

Conflicts of Interest: The authors declare no conflict of interest.

References

1. Sies, H. Oxidative Stress: A Concept in Redox Biology and Medicine. *Redox Biol.* **2015**, *4*, 180–183. [CrossRef]
2. Cadenas, E.; Davies, K.J.A. Mitochondrial Free Radical Generation, Oxidative Stress, and Aging. *Free Radic. Biol. Med.* **2000**, *29*, 222–230. [CrossRef]
3. Lewis, D.F. Oxidative Stress: The Role of Cytochromes P450 in Oxygen Activation. *J. Chem. Technol. Biotechnol.* **2002**, *77*, 1095–1100. [CrossRef]
4. Flohé, L. Glutathione Peroxidase: Fact and Fiction. *Ciba Found. Symp.* **1978**, *65*, 95–122.
5. Barnham, K.J.; Masters, C.L.; Bush, A.I. Neurodegenerative Diseases and Oxidative Stress. *Nat. Rev. Drug Discov.* **2004**, *3*, 205–214. [CrossRef]
6. Dubois-Deruy, E.; Peugnet, V.; Turkieh, A.; Pinet, F. Oxidative Stress in Cardiovascular Diseases. *Antioxidants* **2020**, *9*, 864. [CrossRef]
7. Klaunig, J.E. Oxidative Stress and Cancer. *Curr. Pharm. Des.* **2019**, *24*, 4771–4778. [CrossRef]
8. Tobe, E. Mitochondrial Dysfunction, Oxidative Stress, and Major Depressive Disorder. *Neuropsychiatr. Dis. Treat.* **2013**, *9*, 567. [CrossRef]
9. Emiliani, F.E.; Sedlak, T.W.; Sawa, A. Oxidative Stress and Schizophrenia. *Curr. Opin. Psychiatry* **2014**, *27*, 185–190. [CrossRef] [PubMed]
10. Gassen, M.; Youdim, M.B.H. Free Radical Scavengers: Chemical Concepts and Clinical Relevance. *J. Neural. Transm. Suppl.* **1999**, *56*, 193–210. [CrossRef]
11. Eleutherio, E.C.A.; Silva Magalhães, R.S.; de Araújo Brasil, A.; Monteiro Neto, J.R.; de Holanda Paranhos, L. SOD1, More than Just an Antioxidant. *Arch. Biochem. Biophys.* **2021**, *697*, 108701. [CrossRef] [PubMed]
12. Flohé, L.; Toppo, S.; Orian, L. The Glutathione Peroxidase Family: Discoveries and Mechanism. *Free Radic. Biol. Med.* **2022**, *187*, 113–122. [CrossRef] [PubMed]
13. Orian, L.; Flohé, L. Selenium-Catalyzed Reduction of Hydroperoxides in Chemistry and Biology. *Antioxidants* **2021**, *10*, 1560. [CrossRef]
14. Deisseroth, A.; Dounce, A.L. Catalase: Physical and Chemical Properties, Mechanism of Catalysis, and Physiological Role. *Physiol. Rev.* **1970**, *50*, 319–375. [CrossRef] [PubMed]
15. Labunskyy, V.M.; Hatfield, D.L.; Gladyshev, V.N. Selenoproteins: Molecular Pathways and Physiological Roles. *Physiol. Rev.* **2014**, *94*, 739–777. [CrossRef] [PubMed]
16. Galano, A.; Mazzone, G.; Alvarez-Diduk, R.; Marino, T.; Alvarez-Idaboy, J.R.; Russo, N. Food Antioxidants: Chemical Insights at the Molecular Level. *Annu. Rev. Food Sci. Technol.* **2016**, *7*, 335–352. [CrossRef]
17. Galano, A.; Tan, D.X.; Reiter, R.J. Melatonin as a Natural Ally against Oxidative Stress: A Physicochemical Examination. *J. Pineal. Res.* **2011**, *51*, 1–16. [CrossRef]

18. Shen, N.; Wang, T.; Gan, Q.; Liu, S.; Wang, L.; Jin, B. Plant Flavonoids: Classification, Distribution, Biosynthesis, and Antioxidant Activity. *Food Chem.* **2022**, *383*, 132531. [CrossRef]
19. Yoshida, Y.; Saito, Y.; Jones, L.S.; Shigeri, Y. Chemical Reactivities and Physical Effects in Comparison between Tocopherols and Tocotrienols: Physiological Significance and Prospects as Antioxidants. *J. Biosci. Bioeng.* **2007**, *104*, 439–445. [CrossRef]
20. Cerezo, J.; Zúñiga, J.; Bastida, A.; Requena, A.; Cerón-Carrasco, J.P.; Eriksson, L.A. Antioxidant Properties of β-Carotene Isomers and Their Role in Photosystems: Insights from Ab Initio Simulations. *J. Phys. Chem. A* **2012**, *116*, 3498–3506. [CrossRef]
21. Najafi, H.; Changizi-Ashtiyani, S.; Najafi, M. Antioxidant Activity of Omega-3 Derivatives and Their Delivery via Nanocages and Nanocones: DFT and Experimental in Vivo Investigation. *J. Mol. Model.* **2017**, *23*, 326. [CrossRef] [PubMed]
22. Ahmadvand, H.; Mabuchi, H.; Nohara, A.; Kobayahi, J.; Kawashiri, M. Effects of Coenzyme Q(10) on LDL Oxidation in Vitro. *Acta Med. Iran.* **2013**, *51*, 12–18.
23. Aldini, G.; Altomare, A.; Baron, G.; Vistoli, G.; Carini, M.; Borsani, L.; Sergio, F. N-Acetylcysteine as an Antioxidant and Disulphide Breaking Agent: The Reasons Why. *Free Radic. Res.* **2018**, *52*, 751–762. [CrossRef] [PubMed]
24. Zeppilli, D.; Ribaudo, G.; Pompermaier, N.; Madabeni, A.; Bortoli, M.; Orian, L. Radical Scavenging Potential of Ginkgolides and Bilobalide: Insight from Molecular Modeling. *Antioxidants* **2023**, *12*, 525. [CrossRef] [PubMed]
25. Njus, D.; Kelley, P.M.; Tu, Y.-J.; Schlegel, H.B. Ascorbic Acid: The Chemistry Underlying Its Antioxidant Properties. *Free Radic. Biol. Med.* **2020**, *159*, 37–43. [CrossRef] [PubMed]
26. Sun, C.; Liu, Y.; Zhan, L.; Rayat, G.R.; Xiao, J.; Jiang, H.; Li, X.; Chen, K. Anti-Diabetic Effects of Natural Antioxidants from Fruits. *Trends Food Sci. Technol.* **2021**, *117*, 3–14. [CrossRef]
27. Zhao, C.-N.; Meng, X.; Li, Y.; Li, S.; Liu, Q.; Tang, G.-Y.; Li, H.-B. Fruits for Prevention and Treatment of Cardiovascular Diseases. *Nutrients* **2017**, *9*, 598. [CrossRef] [PubMed]
28. Pillai, A. Brain-Derived Neurotropic Factor/TrkB Signaling in the Pathogenesis and Novel Pharmacotherapy of Schizophrenia. *Neurosignals* **2008**, *16*, 183–193. [CrossRef] [PubMed]
29. Williams, R.J.; Spencer, J.P.E.; Rice-Evans, C. Flavonoids: Antioxidants or Signalling Molecules? *Free Radic. Biol. Med.* **2004**, *36*, 838–849. [CrossRef]
30. Ahmed, S.; Sulaiman, S.A.; Baig, A.A.; Ibrahim, M.; Liaqat, S.; Fatima, S.; Jabeen, S.; Shamim, N.; Othman, N.H. Honey as a Potential Natural Antioxidant Medicine: An Insight into Its Molecular Mechanisms of Action. *Oxid. Med. Cell. Longev.* **2018**, *2018*, 8367846. [CrossRef]
31. Ho, H.-H.; Chang, C.-S.; Ho, W.-C.; Liao, S.-Y.; Wu, C.-H.; Wang, C.-J. Anti-Metastasis Effects of Gallic Acid on Gastric Cancer Cells Involves Inhibition of NF-KB Activity and Downregulation of PI3K/AKT/Small GTPase Signals. *Food Chem. Toxicol.* **2010**, *48*, 2508–2516. [CrossRef] [PubMed]
32. Meshkibaf, M.H.; Maleknia, M.; Noroozi, S. Effect of Curcumin on Gene Expression and Protein Level of Methionine Sulfoxide Reductase A (MSRA), SOD, CAT and GPx in Freund's Adjuvant Inflammation-Induced Male Rats. *J. Inflamm. Res.* **2019**, *12*, 241–249. [CrossRef] [PubMed]
33. Calabrese, V.; Cornelius, C.; Trovato-Salinaro, A.; Cambria, M.; Locascio, M.; Rienzo, L.; Condorelli, D.; Mancuso, C.; De Lorenzo, A.; Calabrese, E. The Hormetic Role of Dietary Antioxidants in Free Radical-Related Diseases. *Curr. Pharm. Des.* **2010**, *16*, 877–883. [CrossRef] [PubMed]
34. Hrelia, S.; Angeloni, C. New Mechanisms of Action of Natural Antioxidants in Health and Disease. *Antioxidants* **2020**, *9*, 344. [CrossRef]
35. Khan, M.S.; Ikram, M.; Park, J.S.; Park, T.J.; Kim, M.O. Gut Microbiota, Its Role in Induction of Alzheimer's Disease Pathology, and Possible Therapeutic Interventions: Special Focus on Anthocyanins. *Cells* **2020**, *9*, 853. [CrossRef]
36. Mantovani, G.; Madeddu, C.; Macciò, A.; Gramignano, G.; Lusso, M.R.; Massa, E.; Astara, G.; Serpe, R. Cancer-Related Anorexia/Cachexia Syndrome and Oxidative Stress: An Innovative Approach beyond Current Treatment. *Cancer Epidemiol. Biomark. Prev.* **2004**, *13*, 1651–1659. [CrossRef]
37. Shinn, L.J.; Lagalwar, S. Treating Neurodegenerative Disease with Antioxidants: Efficacy of the Bioactive Phenol Resveratrol and Mitochondrial-Targeted MitoQ and SkQ. *Antioxidants* **2021**, *10*, 573. [CrossRef]
38. Speer, H.; D'Cunha, N.M.; Alexopoulos, N.I.; McKune, A.J.; Naumovski, N. Anthocyanins and Human Health—A Focus on Oxidative Stress, Inflammation and Disease. *Antioxidants* **2020**, *9*, 366. [CrossRef]
39. Kabuto, H.; Amakawa, M.; Mankura, M.; Yamanushi, T.T.; Mori, A. Docosahexaenoic Acid Ethyl Ester Enhances 6-Hydroxydopamine-Induced Neuronal Damage by Induction of Lipid Peroxidation in Mouse Striatum. *Neurochem. Res.* **2009**, *34*, 1299–1303. [CrossRef]
40. Xu, Y.; Wang, C.; Klabnik, J.; O' Donnell, J. Novel Therapeutic Targets in Depression and Anxiety: Antioxidants as a Candidate Treatment. *Curr. Neuropharmacol.* **2014**, *12*, 108–119. [CrossRef]
41. Ribaudo, G.; Bortoli, M.; Pavan, C.; Zagotto, G.; Orian, L. Antioxidant Potential of Psychotropic Drugs: From Clinical Evidence to In Vitro and In Vivo Assessment and toward a New Challenge for in Silico Molecular Design. *Antioxidants* **2020**, *9*, 714. [CrossRef]
42. Ribaudo, G.; Bortoli, M.; Ongaro, A.; Oselladore, E.; Gianoncelli, A.; Zagotto, G.; Orian, L. Fluoxetine Scaffold to Design Tandem Molecular Antioxidants and Green Catalysts. *RSC Adv.* **2020**, *10*, 18583–18593. [CrossRef] [PubMed]
43. Ribaudo, G.; Bortoli, M.; Witt, C.E.; Parke, B.; Mena, S.; Oselladore, E.; Zagotto, G.; Hashemi, P.; Orian, L. ROS-Scavenging Selenofluoxetine Derivatives Inhibit In Vivo Serotonin Reuptake. *ACS Omega* **2022**, *7*, 8314–8322. [CrossRef] [PubMed]

44. Muraro, C.; Dalla Tiezza, M.; Pavan, C.; Ribaudo, G.; Zagotto, G.; Orian, L. Major Depressive Disorder and Oxidative Stress: In Silico Investigation of Fluoxetine Activity against ROS. *Appl. Sci.* **2019**, *9*, 3631. [CrossRef]
45. Bortoli, M.; Dalla Tiezza, M.; Muraro, C.; Pavan, C.; Ribaudo, G.; Rodighiero, A.; Tubaro, C.; Zagotto, G.; Orian, L. Psychiatric Disorders and Oxidative Injury: Antioxidant Effects of Zolpidem Therapy Disclosed In Silico. *Comput. Struct. Biotechnol. J.* **2019**, *17*, 311–318. [CrossRef]
46. sadat Yousefsani, B.; Akbarizadeh, N.; Pourahmad, J. The Antioxidant and Neuroprotective Effects of Zolpidem on Acrylamide-Induced Neurotoxicity Using Wistar Rat Primary Neuronal Cortical Culture. *Toxicol. Rep.* **2020**, *7*, 233–240. [CrossRef]
47. Sabe, V.T.; Ntombela, T.; Jhamba, L.A.; Maguire, G.E.M.; Govender, T.; Naicker, T.; Kruger, H.G. Current Trends in Computer Aided Drug Design and a Highlight of Drugs Discovered via Computational Techniques: A Review. *Eur. J. Med. Chem.* **2021**, *224*, 113705. [CrossRef]
48. Nimse, S.B.; Pal, D. Free Radicals, Natural Antioxidants, and Their Reaction Mechanisms. *RSC Adv.* **2015**, *5*, 27986–28006. [CrossRef]
49. Orian, L.; Toppo, S. Organochalcogen Peroxidase Mimetics as Potential Drugs: A Long Story of a Promise Still Unfulfilled. *Free Radic. Biol. Med.* **2014**, *66*, 65–74. [CrossRef] [PubMed]
50. P Wolters, L.; Orian, L. Peroxidase Activity of Organic Selenides: Mechanistic Insights from Quantum Chemistry. *Curr. Org. Chem.* **2016**, *20*, 189–197. [CrossRef]
51. Dalla Tiezza, M.; Ribaudo, G.; Orian, L. Organodiselenides: Organic Catalysis and Drug Design Learning from Glutathione Peroxidase. *Curr. Org. Chem.* **2019**, *23*, 1381–1402. [CrossRef]
52. Muraro, C.; Polato, M.; Bortoli, M.; Aiolli, F.; Orian, L. Radical Scavenging Activity of Natural Antioxidants and Drugs: Development of a Combined Machine Learning and Quantum Chemistry Protocol. *J. Chem. Phys.* **2020**, *153*, 114117. [CrossRef] [PubMed]
53. Hernández-López, H.; Tejada-Rodríguez, C.J.; Leyva-Ramos, S. A Panoramic Review of Benzimidazole Derivatives and Their Potential Biological Activity. *Mini Rev. Med. Chem.* **2022**, *22*, 1268–1280. [CrossRef] [PubMed]
54. Anastassova, N.; Aluani, D.; Kostadinov, A.; Rangelov, M.; Todorova, N.; Hristova-Avakumova, N.; Argirova, M.; Lumov, N.; Kondeva-Burdina, M.; Tzankova, V.; et al. Evaluation of the Combined Activity of Benzimidazole Arylhydrazones as New Anti-Parkinsonian Agents: Monoamine Oxidase-B Inhibition, Neuroprotection and Oxidative Stress Modulation. *Neural Regen. Res.* **2021**, *16*, 2299–2309. [CrossRef]
55. Imran, M.; Shah, F.A.; Nadeem, H.; Zeb, A.; Faheem, M.; Naz, S.; Bukhari, A.; Ali, T.; Li, S. Synthesis and Biological Evaluation of Benzimidazole Derivatives as Potential Neuroprotective Agents in an Ethanol-Induced Rodent Model. *ACS Chem. Neurosci.* **2021**, *12*, 489–505. [CrossRef]
56. Ullah, A.; Al Kury, L.T.; Althobaiti, Y.S.; Ali, T.; Shah, F.A. Benzimidazole Derivatives as New Potential NLRP3 Inflammasome Inhibitors That Provide Neuroprotection in a Rodent Model of Neurodegeneration and Memory Impairment. *J. Inflamm. Res.* **2022**, *15*, 3873–3890. [CrossRef]
57. Aleyasin, H.; Karuppagounder, S.S.; Kumar, A.; Sleiman, S.; Basso, M.; Ma, T.; Siddiq, A.; Chinta, S.J.; Brochier, C.; Langley, B.; et al. Antihelminthic Benzimidazoles Are Novel HIF Activators That Prevent Oxidative Neuronal Death via Binding to Tubulin. *Antioxid. Redox Signal.* **2015**, *22*, 121–134. [CrossRef]
58. Yadav, G.; Ganguly, S. Structure Activity Relationship (SAR) Study of Benzimidazole Scaffold for Different Biological Activities: A Mini-Review. *Eur. J. Med. Chem.* **2015**, *97*, 419–443. [CrossRef]
59. Galano, A.; Reiter, R.J. Melatonin and Its Metabolites vs Oxidative Stress: From Individual Actions to Collective Protection. *J. Pineal. Res.* **2018**, *65*, e12514. [CrossRef]
60. Galano, A.; Raúl Alvarez-Idaboy, J. Computational Strategies for Predicting Free Radical Scavengers' Protection against Oxidative Stress: Where Are We and What Might Follow? *Int. J. Quantum Chem.* **2019**, *119*, 1–23. [CrossRef]
61. Ribaudo, G.; Bellanda, M.; Menegazzo, I.; Wolters, L.P.; Bortoli, M.; Ferrer-Sueta, G.; Zagotto, G.; Orian, L. Mechanistic Insight into the Oxidation of Organic Phenylselenides by H_2O_2. *Chem. Eur. J.* **2017**, *23*, 2405–2422. [CrossRef]
62. Ribaudo, G.; Bortoli, M.; Oselladore, E.; Ongaro, A.; Gianoncelli, A.; Zagotto, G.; Orian, L. Selenoxide Elimination Triggers Enamine Hydrolysis to Primary and Secondary Amines: A Combined Experimental and Theoretical Investigation. *Molecules* **2021**, *26*, 2770. [CrossRef]
63. Teixeira Rocha, J.B.; Nogara, P.A.A.; Pereira, M.E.; Sirlene de Oliveira, C.; Orian, L. Organic Selenocompounds: Are They the Panacea to Human Illnesses? *New J. Chem.* **2023**. [CrossRef]
64. Ott, I. Metal N-Heterocyclic Carbene Complexes in Medicinal Chemistry. In *Advances in Inorganic Chemistry*; Academic Press: Cambridge, MA, USA, 2020; Volume 75, pp. 121–148.
65. Tialiou, A.; Chin, J.; Keppler, B.K.; Reithofer, M.R. Current Developments of N-Heterocyclic Carbene Au(I)/Au(III) Complexes toward Cancer Treatment. *Biomedicines* **2022**, *10*, 1417. [CrossRef] [PubMed]
66. Porchia, M.; Pellei, M.; Marinelli, M.; Tisato, F.; Del Bello, F.; Santini, C. New Insights in Au-NHCs Complexes as Anticancer Agents. *Eur. J. Med. Chem.* **2018**, *146*, 709–746. [CrossRef] [PubMed]
67. Mora, M.; Gimeno, M.C.; Visbal, R. Recent Advances in Gold–NHC Complexes with Biological Properties. *Chem. Soc. Rev.* **2019**, *48*, 447–462. [CrossRef] [PubMed]
68. Alberto, E.E.; Rossato, L.L.; Alves, S.H.; Alves, D.; Braga, A.L. Imidazolium Ionic Liquids Containing Selenium: Synthesis and Antimicrobial Activity. *Org. Biomol. Chem.* **2011**, *9*, 1001–1003. [CrossRef]

69. Klauke, K.; Gruber, I.; Knedel, T.-O.; Schmolke, L.; Barthel, J.; Breitzke, H.; Buntkowsky, G.; Janiak, C. Silver, Gold, Palladium, and Platinum N-Heterocyclic Carbene Complexes Containing a Selenoether-Functionalized Imidazol-2-Ylidene Moiety. *Organometallics* **2018**, *37*, 298–308. [CrossRef]
70. Sharma, K.N.; Joshi, H.; Sharma, A.K.; Prakash, O.; Singh, A.K. Selenium-Containing N-Heterocyclic Carbenes and Their First Palladium(II) Complexes: Synthesis, Structure, and Pendent Alkyl Chain Length Dependent Catalytic Activity for Suzuki–Miyaura Coupling. *Organometallics* **2013**, *32*, 2443–2451. [CrossRef]
71. Bhaskar, R.; Sharma, A.K.; Singh, A.K. Palladium(II) Complexes of N-Heterocyclic Carbene Amidates Derived from Chalcogenated Acetamide-Functionalized 1 H-Benzimidazolium Salts: Recyclable Catalyst for Regioselective Arylation of Imidazoles under Aerobic Conditions. *Organometallics* **2018**, *37*, 2669–2681. [CrossRef]
72. Klauke, K.; Zaitsau, D.H.; Bülow, M.; He, L.; Klopotowski, M.; Knedel, T.-O.; Barthel, J.; Held, C.; Verevkin, S.P.; Janiak, C. Thermodynamic Properties of Selenoether-Functionalized Ionic Liquids and Their Use for the Synthesis of Zinc Selenide Nanoparticles. *Dalton Trans.* **2018**, *47*, 5083–5097. [CrossRef]
73. Dubey, P.; Singh, A.K. Sonogashira Coupling (Cu/Amine-Free) of ArBr/Cl in Aerobic Condition and N-Benzylation of Aniline with Benzyl Alcohol Catalyzed by Complexes of Pd(II) with Sulfated/Selenated NHCs. *ChemistrySelect* **2020**, *5*, 2925–2934. [CrossRef]
74. Dubey, P.; Gupta, S.; Singh, A.K. Trinuclear Complexes of Palladium(II) with Chalcogenated N-Heterocyclic Carbenes: Catalysis of Selective Nitrile–Primary Amide Interconversion and Sonogashira Coupling. *Dalton Trans.* **2017**, *46*, 13065–13076. [CrossRef] [PubMed]
75. Kumari, S.; Sharma, C.; Satrawala, N.; Srivastava, A.K.; Sharma, K.N.; Joshi, R.K. Selenium-Directed *Ortho* C–H Activation of Benzyl Selenide by a Selenated NHC–Half-Pincer Ruthenium(II) Complex. *Organometallics* **2022**, *41*, 1403–1411. [CrossRef]
76. Khandaka, H.; Kumar Joshi, R. Fe3O4@SiO2Supported Pd (II)-Selenoether N-Heterocyclic Carbene: A Highly Active and Reusable Heterogeneous Catalyst for C O Cross-Coupling of Alcohols and Chloroarenes. *Tetrahedron Lett.* **2022**, *111*, 154163. [CrossRef]
77. Tishchenko, O.; Truhlar, D.G.; Ceulemans, A.; Nguyen, M.T. A Unified Perspective on the Hydrogen Atom Transfer and Proton-Coupled Electron Transfer Mechanisms in Terms of Topographic Features of the Ground and Excited Potential Energy Surfaces As Exemplified by the Reaction between Phenol and Radicals. *J. Am. Chem. Soc.* **2008**, *130*, 7000–7010. [CrossRef] [PubMed]
78. Draganić, I.G.; Draganićs, Z.D. *The Radiation Chemistry of Water*; Academic Press: New York, NY, USA, 1971; ISBN 9780323158787.
79. Haber, F.; Weiss, J.; Seph, J.O.; Eiss, W. The Catalytic Decomposition of Hydrogen Peroxide by Iron Salts. *Proc. Math. Phys. Sci.* **1934**, *147*, 332–351. [CrossRef]
80. Halliwell, B. Superoxide-Dependent Formation of Hydroxyl Radicals in the Presence of Iron Chelates. *FEBS Lett.* **1978**, *92*, 321–326. [CrossRef] [PubMed]
81. Jiménez, E.; Gilles, M.K.; Ravishankara, A.R. Kinetics of the Reactions of the Hydroxyl Radical with CH_3OH and C_2H_5OH between 235 and 360 K. *J. Photochem. Photobiol. A Chem.* **2003**, *157*, 237–245. [CrossRef]
82. Pryor, W.A. Oxy-Radicals and Related Species: Their Formation, Lifetimes, and Reactions. *Annu. Rev. Physiol.* **1986**, *48*, 657–667. [CrossRef]
83. Hamlin, T.A.; Swart, M.; Bickelhaupt, F.M. Nucleophilic Substitution (S_N2): Dependence on Nucleophile, Leaving Group, Central Atom, Substituents, and Solvent. *ChemPhysChem* **2018**, *19*, 1315–1330. [CrossRef]
84. Frisch, M.J.; Trucks, G.W.; Schlegel, H.B.; Scuseria, G.E.; Robb, M.A.; Cheeseman, J.R.; Scalmani, G.; Barone, V.; Petersson, G.A.; Nakatsuji, H.; et al. *Gaussian 16, Revision B.01*; Gaussian, Inc.: Wallingford, CT, USA, 2016.
85. Zhao, Y.; Truhlar, D.G. The M06 Suite of Density Functionals for Main Group Thermochemistry, Thermochemical Kinetics, Noncovalent Interactions, Excited States, and Transition Elements: Two New Functionals and Systematic Testing of Four M06-Class Functionals and 12 Other Functionals. *Theor. Chem. Acc.* **2008**, *120*, 215–241. [CrossRef]
86. Marenich, A.V.; Cramer, C.J.; Truhlar, D.G. Universal Solvation Model Based on Solute Electron Density and on a Continuum Model of the Solvent Defined by the Bulk Dielectric Constant and Atomic Surface Tensions. *J. Phys. Chem. B* **2009**, *113*, 6378–6396. [CrossRef] [PubMed]
87. *ADF2016 SCM. Theoretical Chemistry*; Vrije Universiteit: Amsterdam, The Netherlands, 2016; Available online: https://www.scm.com/ (accessed on 26 June 2023).
88. van Lenthe, E.; Baerends, E.J.; Snijders, J.G. Relativistic Total Energy Using Regular Approximations. *J. Chem. Phys.* **1994**, *101*, 9783–9792. [CrossRef]
89. Becke, A.D. Density-Functional Exchange-Energy Approximation with Correct Asymptotic Behavior. *Phys. Rev. A* **1988**, *38*, 3098–3100. [CrossRef]
90. Lee, C.; Yang, W.; Parr, R.G. Development of the Colle-Salvetti Correlation-Energy Formula into a Functional of the Electron Density. *Phys. Rev. B* **1988**, *37*, 785–789. [CrossRef] [PubMed]
91. Grimme, S.; Ehrlich, S.; Goerigk, L. Effect of the Damping Function in Dispersion Corrected Density Functional Theory. *J. Comput. Chem.* **2011**, *32*, 1456–1465. [CrossRef]
92. Becke, A.D.; Johnson, E.R. A Density-Functional Model of the Dispersion Interaction. *J. Chem. Phys.* **2005**, *123*, 154101. [CrossRef]

93. Figgen, D.; Rauhut, G.; Dolg, M.; Stoll, H. Energy-Consistent Pseudopotentials for Group 11 and 12 Atoms: Adjustment to Multi-Configuration Dirac–Hartree–Fock Data. *Chem. Phys.* **2005**, *311*, 227–244. [CrossRef]
94. Hanwell, M.D.; Curtis, D.E.; Lonie, D.C.; Vandermeersch, T.; Zurek, E.; Hutchison, G.R. Avogadro: An Advanced Semantic Chemical Editor, Visualization, and Analysis Platform. *J. Cheminform.* **2012**, *4*, 17. [CrossRef]